Opacity and Transport Measurements Reveal That Dilute Plasma Models of Sonoluminescence Are Not Valid

Shahzad Khalid,[1] Brian Kappus,[1] Keith Weninger,[2] and Seth Putterman[1]
[1]*Department of Physics and Astronomy, University of California, Los Angeles, Los Angeles, California, USA*
[2]*Department of Physics, North Carolina State University, Raleigh, North Carolina, USA*
(Received 3 May 2011; published 6 March 2012)

A strong interaction between a nanosecond laser and a 70 μm radius sonoluminescing plasma is achieved. The overall response of the system results in a factor of 2 increase in temperature as determined by its spectrum. Images of the interaction reveal that light energy is absorbed and trapped in a region smaller than the sonoluminescence emitting region of the bubble for over 100 ns. We interpret this opacity and transport measurement as demonstrating that sonoluminescencing bubbles can be 1000 times more opaque than what follows from the Saha equation of statistical mechanics in the ideal plasma limit. To address this discrepancy, we suggest that the effects of strong Coulomb interactions are an essential component of a first principles theory of sonoluminescence.

DOI: 10.1103/PhysRevLett.108.104302 PACS numbers: 78.60.Mq, 43.25.+y

Sonoluminescence (SL) is the emission of light from a gas bubble that is driven by a sound field to pulsate at high amplitude. The bubble expands during the rarefaction part of the cycle, and implodes subsequently to emit a flash of light. The fluid dynamics of how the sound field creates these pulsations is, to a good approximation, explained by the Raleigh-Plesset equation [1]. Furthermore, it is generally accepted that the gas in the collapsed bubble becomes so hot that it forms a plasma, and that light emission has its origin in accelerating electrons in this plasma [2–5]. However, the properties of this plasma such as its degree of ionization and opacity is the subject of varying opinions. Some have argued that ionized density is so low that the plasma is nearly transparent [3,4]. However, this conflicts with the observation that SL emission is best fit by Planck's law for an opaque blackbody and not a bremsstrahlung spectrum from a transparent plasma [5]. An analysis of spectral lines [6], a comparison of the measured physical radius to spectrally extracted radius [7], and a numerical model [8] also suggest an ionization level that is much higher than would be consistent with a transparent plasma.

We present the first measurements of the dynamic response of an SL microplasma to the energy contained in a laser pulse. As shown in Fig. 1, we find that the energy delivered by a 3 ns pulse is confined for at least 100 ns to a relatively small fraction of bubble volume which faces the incoming laser. By comparing the images of laser absorption in the bright (Fig. 1) and dim (Fig. 2) phases of the bubble, and by analyzing the minimally heated bubbles (Fig. 3) we argue that the bright SL plasma has high intrinsic opacity. A degree of ionization which is much higher than what follows from the Saha equation is needed to explain this opacity. This underlines the shortcomings of SL models relying on dilute plasma physics and ignoring strong Coulomb interactions.

We chose a liquid hammer tube bubble [9,10] driven at a frequency of 38 Hz because its collapse radius of about 70 μm is 100 times larger than that of a single steady state of SL bubbles driven at 20 to 40 kHz. Cao *et al.* [11] attempted to laser heat a much smaller 23 kHz bubble and found no evidence of laser interaction. The large radius of our bubble allows us to acquire detailed images of the internal structure of the SL plasma. The bubble is trapped and driven in a 24 cm tall quartz tube with 3.6 cm outer diameter and 3 cm inner diameter filled with dehydrated phosphoric acid to a height of 12 cm. The tube is rotated at

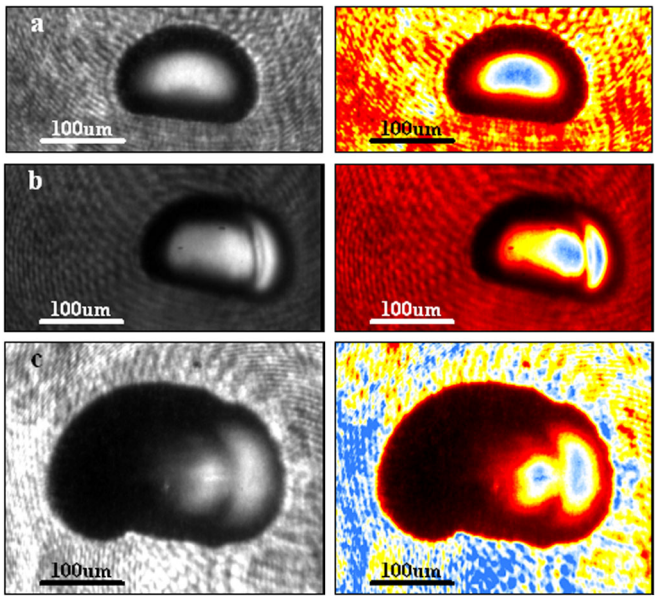

FIG. 1 (color online). Images and their false color versions of a bright bubble with exposure before laser heating (a), 60 ns after laser heating (b), and 360 ns after laser heating (c). Laser is incoming from the right side.

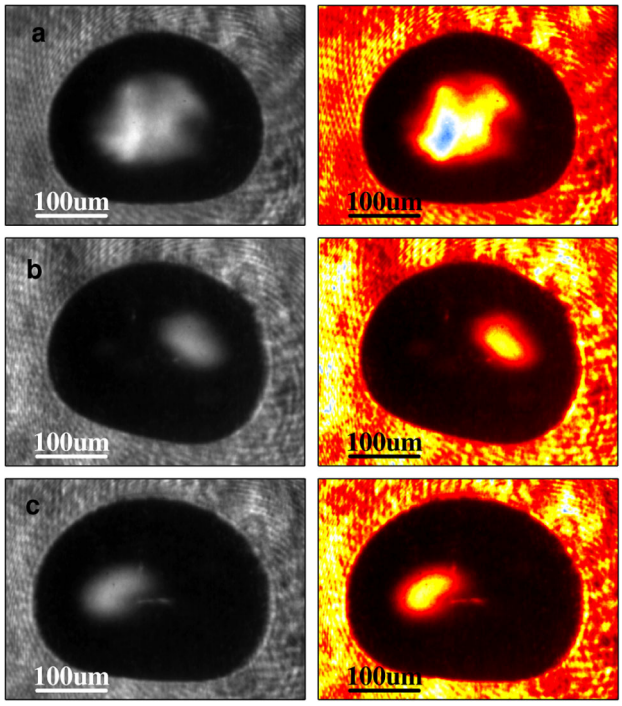

FIG. 2 (color online). Sample images and their false color versions of laser pulse interaction with extremely dim bubbles showing random locations of hot spot. Laser is incoming from the right side.

6.3 Hz to constrain the bubble on the axis and vertically vibrated at 38 Hz by a mechanical shaker with a sinusoidal amplitude of ~1 mm which drives the bubble into SL emitting oscillations while simultaneously trapping it about 2 cm above the bottom of the tube. Our liquid hammer device is similar to the one described in [10–12] except for two key modifications to attain a consistently repeatable bubble [13]. We mix gas and liquid well with 20 torr overhead pressure, and we seed our bubble with a laser pulse. When driven by the shaker, this laser seeded bubble grows due to gas diffusion while getting brighter and then dimmer over a few minutes in a repeatable manner. Application of the ideal gas law to the bubble volume measured from imaging under ambient conditions (without the vertical drive) yields the number of gas atoms. The pressure used in the ideal gas law is calculated by adding the liquid column pressure to the overhead gas pressure of 20 Torr. Dividing the number of atoms by collapse volume gives the collapse density. The uncertainty in the collapse density is mainly due to fluctuations in the ambient bubble radius and the collapse radius. The gas used for the results presented here is Xe, which has a flash width of ~500 ns FWHM and a collapse density of $(4.2 \pm 0.8) \times 10^{20}$ atoms/cm^3. A 3 ns pulse from a 532 nm laser was synchronized to SL by triggering its Q switch from the photomultiplier tube (PMT) signal of SL emission, and was focused to the 45 μm radius in the tube. Our system differs from the liquid hammer setup of Ref. [14] in that there is no extra bubble at the bottom of the tube.

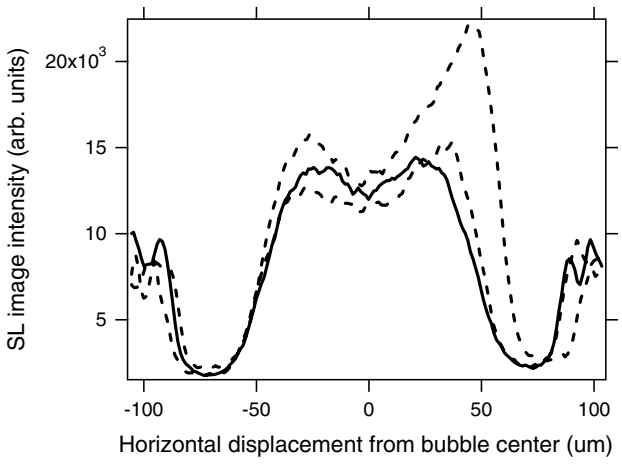

FIG. 3 (color online). Comparison of the horizontal profiles from the images of laser heated bright bubbles. The solid curve is an unheated bright bubble for reference. The dashed curves are minimally heated bubbles by low energy laser pulses of 1.2 mJ (upper) and 1.0 mJ (lower). Laser is incoming from the right side.

Imaging resolution was enhanced by fabrication of high precision quartz tubes and custom corrective optics. All images are taken with an intensified CCD with a 100 ns exposure. Figure 1(a) shows a typical image of an unheated bright bubble at its collapse radius. The false color version is on the right panel. Background light arises from a 532 nm cw external illumination of the bubble. Refraction of this backlighting away from the imaging optics makes the bubble wall visible in the image. Since the refractive index of the liquid is higher than the gas inside the bubble, the image of SL emission has a dark region at its outer edges in Fig. 1(a) due to bending of SL rays as they pass through the gas liquid interface. Figure 1(b) shows a typical image acquired just after single pulse laser heating of a bright bubble. The ''bright'' phase of the bubble exists about ±300 ns around the minimum radius. Laser absorption occurs mainly in the side of SL facing the incoming laser. The heated right side in Fig. 1(b) has two distinct hot spots. The hot spot closer to the center is the laser heated version of SL. The hot spot near the edge is a new extended region of plasma created by the laser. This image can be explained by refraction effects: When the laser energizes SL at the edge, a protruding semispherical surface is created due to plasma expansion. The curvature of this bump refracts this new plasma light into imaging optics, and thus makes the second hot spot near the edge as seen in Fig. 1(b). In other words, a single bright area near the bubble edge appears as two hot spots in the image. The thin dark strip between the two hot spots can be explained in terms of the curvature of the respective boundaries.

The bump in the bubble wall is even more obvious in Fig. 1(c), which can be viewed as a 300 ns delayed version of Fig. 1(b). Figures 1(b) and 1(c) are acquired from two separate laser heating events, but they represent a typical set of images after hitting a bright SL bubble. Images of laser heated bright bubbles [15] with laser pulse energies of less than 1.5 mJ do not display the second hot spot due to the bump. The plasma heating is gentle enough at these laser energies to avoid significant distortions of the bubble wall. Even at this minimal level of laser heating, the increased intensity is present only on the side facing the incoming laser [15].

In sharp contrast to bright bubbles where laser heating always occurs on the side of the SL microplasma that faces the laser, laser interaction in an extremely dim bubble occurs randomly at different locations as shown in Fig. 2. This "extremely dim" phase of the bubble exists about 0.5–1 μs after the minimum radius is achieved. The randomness in the location of laser interaction with the extremely dim bubble is due to spatial jitter of the bubble and the random nature of laser induced breakdown [16]. The observation of laser created hot spots in the left side of the bubbles in Fig. 2 implies that the extremely dim bubble is transparent enough for the laser to propagate through to its left side. More importantly, it implies that the observed lack of laser propagation in a bright bubble is due to its intrinsic opacity rather than a laser created opacity. If the bright bubble was intrinsically transparent then its interaction with the laser pulse would have resulted in hot spots appearing, at least occasionally, away from the edge facing the incoming laser. This is the key point of this Letter and allows us to place an upper bound on the intrinsic photon mean free path in the bright bubble.

As additional but equally strong evidence of intrinsically high opacity of the bright bubble, Fig. 3 compares the horizontal image profiles of bright bubbles heated by low energy laser pulses to an unheated bright bubble profile. The temperature increase in these minimally heated bright bubbles is less than 10% as measured by their spectra (from 10 000 K to 11 000 K). This means that the plasma state is approximately the same as its intrinsic state with a very small perturbation by the laser. Yet, the increased intensity is only present on the right side facing the laser and the intensity on the left side is comparable to the unheated intensity given shot to shot variations. Again, this implies that the intrinsic opacity of the bright bubble is high enough to prevent laser transmission to the left half of the bubble. This means that the mean free path of a laser photon in the bright bubble plasma at a temperature of (10 500 $\pm$ 500) K is less than the bubble's horizontal radius of 85 μm.

The spectra captured after laser heating events are used to quantify intensity and temperature gains. The plus markers in Fig. 4 show measured intensities (top panel) and Planck fit temperatures (bottom panel) as a function of laser pulse energy. Each marker represents a single event of laser heating of a sonoluminescing bubble. The data are from 17 runs. The intensities are calculated by integrating the measured spectra from 318 to 500 nm. The exposure on the spectrometer's intensified CCD was 10 ns long and was taken 10 ns after the end of the laser pulse. The vertical spread in data is due to spatial jitter in the bubble location relative to the laser and the horizontal spread is due to controlled changes and random fluctuations in laser pulse energy. The top envelope of this data clearly shows that intensity and temperature increase with increasing laser pulse energy up to ~3.5 mJ and then fall off, which is due to breakdown of liquid that prevents laser energy from reaching the bubble. Liquid breakdown is confirmed by images showing appearance of tiny bubbles of less than 4 μm radius near the SL bubble. Furthermore, these tiny bubbles are sucked into the main bubble and temporarily

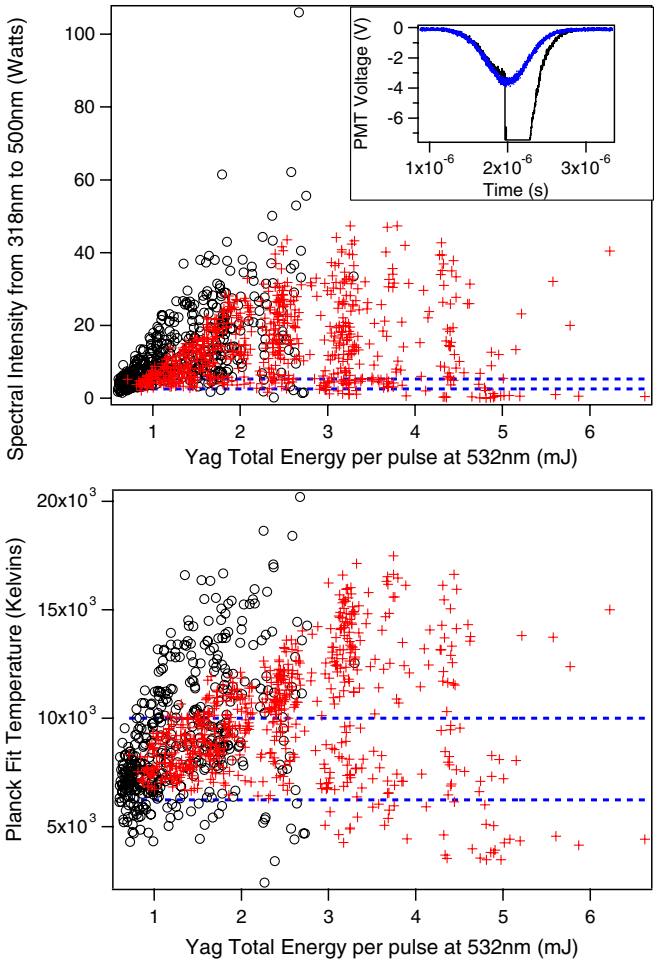

FIG. 4 (color online). Intensity (top) and temperature (bottom) of laser heated bubbles (plus markers in red) as a function of laser energy. Black circles represent data from 8 pulse heatings. Horizontal dashed lines represent the range for unheated bubbles. The inset compares PMT signals of heated (black) and unheated (blue) bubbles.

make it dimmer for up to several seconds, thus explaining the points below the lower dashed lines in Fig. 4.

Identification of liquid breakdown as a limiting factor to the delivery of energy to SL bubbles motivated us to build a beam stretcher with beam splitters and delay paths. The result was a train of 8 pulses of equal energy whose peaks were 3 to 4 ns apart from each other. If each pulse of energy is below the liquid breakdown threshold and alignment is perfect, this arrangement could deliver up to 8 times the energy of a single pulse. The circular markers in Fig. 4 show that 8 pulses deliver more energy to the SL plasma. Relative to the unheated bubble, the peak intensity of 100 W is 20 times brighter, and the peak temperature of 20 200 K is twice as hot. The inset in Fig. 4 shows examples of temporal behavior of SL pulse with and without laser heating captured with a PMT. A 450 nm short pass filter to block the laser was placed in front of the PMT in addition to an OD3 neutral density filter.

The broadband spectra [15] of heated and unheated bright bubbles have no lines, which is consistent with the blackbody emission. A high degree of opacity means that Planck fits to the spectra provide a reasonable estimate for the electron temperature. The spectral data fit rather well [15] to Planck's equation providing temperature estimates with an uncertainty of less than ± 100 K. We note that the dim unheated bubbles have Xe^* lines present at 825 nm as documented in [10].

The observed upper bound of 85 μm on the photon mean free path in a bright bubble with minimal laser heating can be used to estimate a lower bound for its degree of ionization. The Kramers equation [17] for bremsstrahlung absorption due to free-free interactions between electrons and ions relates the photon mean free path l_ν to the degree of ionization α:

$$l_\nu = C_1 \frac{\sqrt{T_e}\nu^3}{\alpha^2 n^2} \tag{1}$$

where T_e is the electron temperature, ν the photon frequency, n the density of atoms including ions, and $C_1 = \sqrt{3m_e k_B}3hcm_e(4\pi\epsilon_0)^3/4\sqrt{2\pi}e^6$ is a function of electron mass m_e, Boltzmann constant k_B, Planck constant h, speed of light c, free space permittivity ϵ_0, and electronic charge e. Using $T_e = (10\,500 \pm 500)$ K, $n = (4.2 \pm 0.8) \times 10^{20}$ cm^{-3}, and $l_\nu \leq 85$ μm we calculate a minimum of $(19 \pm 4)\%$ degree of ionization for 532 nm photons. Including free-bound and free-neutral mechanisms of absorption does not change this requirement significantly. Furthermore, Eq. (1) is applicable because the laser frequency is much higher than the plasma frequency. At $(19 \pm 4)\%$ ionization, the laser frequency is (7 ± 2) times the plasma frequency.

For a dilute gas in thermal equilibrium, the degree of ionization α is related to its temperature T by the Saha equation [17]:

$$\frac{\alpha^2}{1-\alpha} = 2\frac{u_1}{u_0}\frac{1}{n\lambda_e^3}e^{-I/k_BT} \tag{2}$$

where $\lambda_e = h/\sqrt{2\pi m_e k_B T}$ is the electron thermal de Broglie wavelength, I is ionization energy, and u_1/u_0 is the ratio of ionic to atomic electronic partition functions. Using $T = (10\,500 \pm 500)$ K, $n = (4.2 \pm 0.8) \times 10^{20}$ cm^{-3}, $I = 12.1$ eV, and $u_1/u_0 = (2.95 \pm 0.07)$ for our Xe bubble, we calculate a degree of ionization of only $(0.7 \pm 0.4)\%$, which is much smaller than the minimum requirement of $(19 \pm 4)\%$ computed above. The photon mean free path is 60 mm for 0.7% ionization, which is about 1000 times bigger than the observed limit of $l_\nu \leq 85$ μm. Furthermore, a first order correction to the Saha equation by the Debye-Huckel method yields only a 0.3% increase in ionization [15].

This large discrepancy between degree of ionization calculated from the Saha equation and what is required to achieve opacity is strong evidence of inapplicability of the dilute gas plasma model. At $T = (10500 \pm 500)$ K, $n = (4.2 \pm 0.8) \times 10^{20}$ cm^{-3}, and $(19 \pm 4)\%$ ionization, the Coulomb coupling parameter (Γ), which is the ratio of Coulomb energy between neighboring particles to their thermal energy, is (1.1 ± 0.2). If the intrinsic opacity of a bright bubble is due to a high level of ionization, Coulomb interactions play a dominant role in determining the behavior of an SL plasma.

Thermal relaxation times as a function of the degree of ionization can be estimated [15] by considering heat diffusion due to electrons and photons. Results of these calculations show that the thermal relaxation times using our plasma parameters are of the order of a microsecond even at high degrees of ionization. Therefore a high degree of ionization is not in conflict with the observed persistence of thermal gradients in the images of the laser heated bubbles.

We have described an experimental technique capable of time and space resolved measurements of the interaction between a laser pulse and a sonoluminescing microplasma. Our analysis shows that the measured gain in the intensity of bright bubbles is not due to laser interaction with a weakly ionized transparent plasma predicted by prominent SL models, but rather due to absorption of laser energy in an intrinsically opaque plasma. If the opacity and emissivity of SL systems is due to high levels of ionization then a complete theory must include Coulomb interactions.

The work is supported by DARPA (MTO) and generous contributions from the Elwood and Stephanie Norris Foundation.

[1] M. S. Plesset and A. Prosperetti, Annu. Rev. Fluid Mech. **9**, 145 (1977).

[2] C. C. Wu and P. H. Roberts, Proc. R. Soc. A **445**, 323 (1994).

[3] L. Frommhold, Phys. Rev. E **58**, 1899 (1998).
[4] S. Hilgenfeldt, S. Grossmann, and D. Lohse, Phys. Fluids **11**, 1318 (1999).
[5] G. Vazquez, C. Camara, S. Putterman, and K. Weninger, Opt. Lett. **26**, 575 (2001).
[6] D. Flannigan and K. Suslick, Nature Phys. **6**, 598 (2010).
[7] B. Kappus, S. Khalid, A. Chakravarty, and S. Putterman, Phys. Rev. Lett. **106**, 234302 (2011).
[8] L. Yuan and P. He, Mod. Phys. Lett. B **19**, 1711 (2005).
[9] C. K. Su, C. Camara, B. Kappus, and S. J. Putterman, Phys. Fluids **15**, 1457 (2003).
[10] A. Chakravarty, T. Georghiou, T. E. Phillipson, and A. J. Walton, Phys. Rev. E **69**, 066317 (2004).
[11] G. Cao, S. Danworaphong, and G. J. Diebold, Eur. Phys. J. Special Topics **153**, 215 (2008).
[12] B. A. Kappus, Ph.D. thesis, UCLA, 2010.
[13] S. Khalid, Ph.D. thesis, UCLA, 2011.
[14] R. Urteaga, P. L. García-Martínez, and F. J. Bonetto, Phys. Rev. E **79**, 016306 (2009).
[15] See Supplemental Material at http://link.aps.org/supplemental/10.1103/PhysRevLett.108.104302 for spectra and images of heated bubbles, thermal transport analysis, and a correction to the Saha equation.
[16] A. Vogel, K. Nahen, D. Theisen, and J. Noack, IEEE J. Sel. Top. Quantum Electron. **2**, 847 (1996).
[17] Y. B. Zel'dovich and Y. P. Raizer, *Physics of Shock Waves and High-Temperature Hydrodynamic Phenomena* (Academic Press, New York, 1966).